Advances in Aircraft and Spacecraft Science, *Vol. 10, No. 4 (2023) 303-315*
https://doi.org/10.12989/aas.2023.10.4.303

Numerical investigation of turbulence models with emphasis on turbulent intensity at low Reynolds number flows

Musavir Bashir[1a], Parvathy Rajendran[*1], Ambareen Khan[1a], Vijayanandh Raja[2a] and Sher Afghan Khan[3b]

[1]*School of Aerospace Engineering*, *Universiti Sains Malaysia*, *Engineering Campus*, *Nibong Tebal*, *Pulau Pinang*, *Malaysia*
[2]*Department of Aeronautical Engineering*, *Kumaraguru College of Technology*, *Coimbatore-641049*, *Tamil Nadu*, *India*
[3]*Department of Mechanical Engineering*, *Faculty of Engineering*, *International Islamic University*, *Kuala Lumpur 53100*, *Selangor*, *Malaysia*

(Received June 22, 2022, Revised July 19, 2023, Accepted August 7, 2023)

Abstract. The primary goal of this research is to investigate flow separation phenomena using various turbulence models. Also investigated are the effects of free-stream turbulence intensity on the flow over a NACA 0018 airfoil. The flow field around a NACA 0018 airfoil has been numerically simulated using RANS at Reynolds numbers ranging from 100,000 to 200,000 and angles of attack (AoA) ranging from 0° to 18° with various inflow conditions. A parametric study is conducted over a range of chord Reynolds numbers for free-stream turbulence intensities from 0.1 % to 0.5 % to understand the effects of each parameter on the suction side laminar separation bubble. The results showed that increasing the free-stream turbulence intensity reduces the length of the separation bubble formed over the suction side of the airfoil, as well as the flow prediction accuracy of each model. These models were used to compare the modeling accuracy and processing time improvements. The K- SST performs well in this simulation for estimating lift coefficients, with only small deviations at larger angles of attack. However, a stall was not predicted by the transition k-kl-omega. When predicting the location of flow reattachment over the airfoil, the transition k-kl-omega model also made some over-predictions. The Cp plots showed that the model generated results more in line with the experimental findings.

Keywords: CFD simulation; NACA 0018 airfoil; Reynolds number; turbulence model; turbulent intensity

1. Introduction

Airfoils are used in various engineering applications, from UAV wings to wind turbine blades to commercial aircraft wings (Mueller and DeLaurier 2003, Lachenal *et al.* 2013, Zhou *et al.* 2017). Airfoils can also be used at various speeds, from leisurely gliders to supersonic combat aircraft. Because engineers have a substantial challenge regarding necessary airfoil performance due to the broad design space over which airfoils are used, several airfoil designs have been

*Corresponding author, Professor, E-mail: aeparvathy@usm.my
[a]Ph.D.
[b]Professor

http://www.techno-press.org/?journal=aas&subpage=7 ISSN: 2287-528X (Print), 2287-5271 (Online)

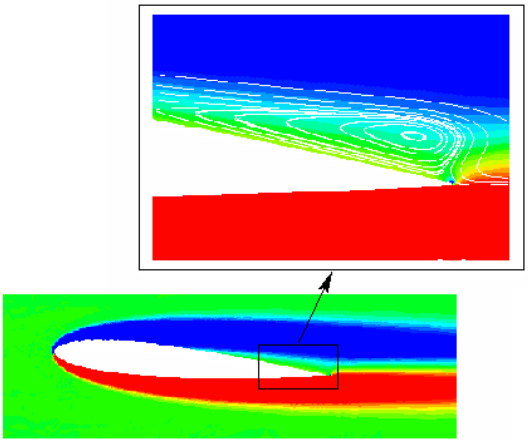

Fig. 1 Instability of separated flow in the trailing edge of standard NACA 0012 airfoil (Theofilis and Sherwin 2001)

thoroughly assessed. The Reynolds number based on the airfoil chord length is an important non-dimensional characteristic that distinguishes this wide range of operating circumstances. One of the most challenging ranges for designing chords is below 700×10^3, where performance drops significantly compared to higher chord Reynolds numbers (Carmichael 1981, Istvan *et al.* 2016). Suction-side laminar boundary layer separation is the primary cause of airfoil performance degradation.

Various qualitative and quantitative experimental techniques have investigated airfoil performance and boundary layer properties at low Reynolds numbers (Drela 1989, Yarusevych *et al.* 2006, Shen *et al.* 2016, Kamada *et al.* 2016). Previous research has shown that the angle of attack and the Reynolds number substantially impact separated shear layer properties over an airfoil. As aerodynamic test models, symmetric airfoils have been widely employed. The NACA 0012 profile is the most researched symmetric airfoil (Gerakopulos *et al*. 2010). McCroskey (Kojima *et al.* 2013) examines experimental aerodynamic performance data from nearly forty different NACA 0012 profile wind tunnel trials, some of which were conducted at low Reynolds numbers. A substantial experimental database is available for a NACA 0015 airfoil and the results for a NACA 0012 profile. Previous research into the effects of vortex shedding, near-wake development, and boundary layer features on an airfoil's aerodynamic performance at low Reynolds numbers has increased our understanding (Gerakopulos *et al*. 2010). In vertical-axis wind and water turbines, thick airfoil sections are necessary to improve blade stiffness. To maintain constant blade loading, somewhat thick symmetric airfoils are required in these applications since the blades oscillate through positive and negative angles of attack (AoA). However, the vast literature available for thin symmetric airfoils with low Reynolds numbers is insufficient for precise design estimations for thicker symmetric airfoils (Kojima *et al.* 2013).

Increasing the Reynolds number reduces the bubble's length when a separation bubble forms on an airfoil's upper surface (O'meara and Mueller 1987). Furthermore, when the angle of attack increases, the laminar separation point moves closer to the leading edge until it stalls. Despite significant efforts to comprehend the evolution of laminar separated shear layers, existing models for describing the separated flow zone on an airfoil still rely on empirically determined criteria and are unreliable. From the perspective of the numerical solution of the two-dimensional partial

derivative eigenvalue problem, Theofilis and Sherwin (2001) investigated the instability of separated flow in the trailing edge of a standard NACA 0012 airfoil. One of the most remarkable properties of the flow at Reynolds number 1000 is trailing-edge separation, as seen in Fig. 1.

There is a reduction in the performance of an airfoil with $Re<700\times10^3$ compared to that of a higher Reynolds number due to a suction side laminar separation bubble (Carmichael 1981). While many distinct airfoil sections have various characteristics for different flow conditions, all airfoils operating in the low Reynolds number zone encounter the laminar separation bubble. At low speeds, the boundary layer developed over the forward zone of the airfoil remains laminar. Thus making it more susceptible to separation than a turbulent boundary layer as it carries minimum momentum near the wall (Jones *et al.* 2018). The flow faces an unfavorable pressure gradient downstream of the suction peak, which may cause the flow to separate. The turbulence that results from the separated shear layer might cause mean flow reattachment due to the increased momentum exchange with the free stream. A laminar separation bubble is a recirculating fluid patch between the mean separation and reattachment points.

There is currently no agreement on the minimal level of flow modeling required to effectively estimate airfoil aerodynamics while considering various flow regimes/states (e.g., laminar, transitional, and turbulent flows) and inflow circumstances (e.g., Reynolds numbers and angles of attack) (Herbert-Acero *et al.* 2015). Consequently, Rogowski *et al.* (2021) have used the conventional uncalibrated four-equation Transition SST turbulence model and the unsteady Reynolds-averaged Navier-Stokes (URANS) equations to assess the aerodynamic performance of the NACA 0018 airfoil and the features of the laminar separation bubble created on its suction side.

The aerodynamic unstable and steady airfoil characteristics of the NACA 0018 airfoil of a two-dimensional vertical-axis wind turbine are described numerically (Rogowski *et al*. 2018) (steady and unsteady). The RNG k- and the SST Transition turbulence models are utilized in this study to analyze the properties of airfoils. The mesh distribution that is utilized around the airfoil edges is the same. The results computed using the SST Transition model correlate quite well with the experiment results, particularly concerning the static airfoil characteristics (Rogowski *et al*. 2018).

Only a few studies have attempted to compare the accuracy of various fluid flow modeling techniques for forecasting the aerodynamic behavior of two-dimensional airfoils under various inflow conditions. The current project's goal is to figure out how separation bubbles behave. Two turbulence models were used in the numerical analysis: the two-equation SST K- and Transition k-kl-omega model. The free stream turbulent intensities are also changed to test the effect at low Reynolds numbers. Finally, the results of the simulation at Reynolds number 120,000 are compared to Gerakopulos et al. experimental investigation (Gerakopulos *et al.* 2010).

2. Governing equation

We consider the RANS equations to be the governing equations for the two-dimensional, unstable, and incompressible flow

$$\frac{\partial \mathrm{u_i}}{\partial \mathrm{x_i}} = 0. \tag{1}$$

$$\frac{\partial \mathrm{u_i}}{\partial \mathrm{t}} + \mathrm{u_j}\frac{\partial \mathrm{u_i}}{\partial \mathrm{x_j}} = -\frac{1}{\rho}\frac{\partial \mathrm{p}}{\partial \mathrm{x_i}} + \upsilon\frac{\partial^2 \mathrm{u_i}}{\partial \mathrm{x_j}\,\partial \mathrm{x_j}} - \frac{\partial \overline{\mathrm{u_i'u_j'}}}{\partial \mathrm{x_j}} \tag{2}$$

where u_i is the mean velocity, v the kinematic viscosity of the air, q the density of air, ρ the pressure, and $-\overline{u_i'}\overline{u_j'}$ the Reynolds stress.

3. Turbulence models

3.1 The SST k-omega turbulence model

The SST *K*-ω combines the Wilcox *K*-ω and the standard *K*-ε model (Menter *et al*. 2003). The standard *K*-ε is transformed to *K*-ω by substituting ε=*K*ω. The turbulent viscosity is defined using the *k*-omega SST turbulence model, which includes the transport of the turbulence shear stress. That is why the *k*-omega SST turbulence model was chosen. *K*-omega SST turbulence model is governed by

$$\frac{D\rho k}{Dt} = \tau_{ij}\frac{\partial u_i}{\partial x_j} + \beta^*\rho\omega k + \frac{\partial}{\partial x_j}\left[(\mu + \sigma_k\mu_t)\frac{\partial k}{\partial x_j}\right] \tag{3}$$

$$\frac{D\rho\omega}{Dt} = \frac{\gamma}{v_t}\tau_{ij}\frac{\partial u_i}{\partial x_j} - \beta\rho\omega^2 + \frac{\partial}{\partial x_j}\left[(\mu + \sigma_k\mu_t)\frac{\partial\omega}{\partial x_j}\right] + 2\rho(1-F_1)\sigma_\omega\frac{1}{\omega}\frac{\partial k}{\partial x_j}\frac{\partial\omega}{\partial x_j} \tag{4}$$

where, β*=$\beta^* = \frac{\varepsilon}{k\omega}$ and the turbulence stress tensor is

$$\tau_{ij} = -\rho\overline{u_i'u_j'} = \mu_t\left(\frac{\partial u_i}{\partial x_j} + \frac{\partial u_j}{\partial x_i} - \frac{2}{3}\frac{\partial u_k}{\partial x_k}\delta_{ij}\right) - \frac{2}{3}\rho k\delta_{ij} \tag{5}$$

The turbulence viscosity can be estimated by $v_t = \frac{a_1 k}{\max(a_1\omega, \Omega F_2)}$, where Ω is the absolute value of the vorticity, a1=0.31 and the function F2 is given by

$$F_2 = \tanh\left\{\left[\max\left(\frac{2\sqrt{k}}{0.09\omega y}, \frac{500v}{y^2\omega}\right)\right]\right\}^2 \tag{6}$$

where y is the distance to the nearest surface.

3.2 The k-kl-ω model

For transition flows, *K*-*kl*-ω was created (Aftab *et al*. 2016, Ghasemi *et al*. 2013) and accurately estimates the boundary layer's transition initiation feature. For turbulent viscosity, three equations are used in this turbulence model.

$$\frac{Dk_T}{D} = P_{K_T} + R + R_{NAT} - \omega k_T - D_T + \frac{\partial}{\partial x_j}\left[\left(v + \frac{\alpha_T}{\alpha_k}\right)\frac{\partial k_T}{\partial x_j}\right] \tag{7}$$

$$\frac{Dk_L}{D_t} = P_{K_L} - R - R_{NAT} - D_L + \frac{\partial}{\partial x_j}\left[v\frac{\partial k_L}{\partial x_j}\right] \tag{8}$$

$$\frac{D_\omega}{D_t} = C_{\omega 1}\frac{\omega}{k_T}P_{K_T} + \left(\frac{C_{\omega R}}{f_W} - 1\right)\frac{\omega}{k_T}(R + R_{NAT}) - C\omega_2\omega^2 + C\omega_3 f_\omega\alpha_T f_W^2\frac{\sqrt{k_T}}{d^3} + \frac{\partial}{\partial x_j}\left[\left(v + \frac{\alpha_\gamma}{\alpha_\omega}\right)\frac{\partial\omega}{\partial x_j}\right] \tag{9}$$

The turbulent kinetic energy is modeled using *KT*. The turbulent kinetic energy is modeled

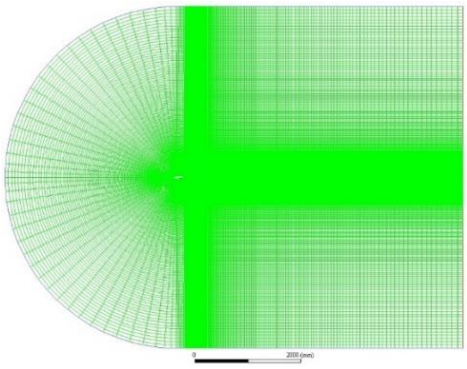

Fig. 2 Domain with structured mesh

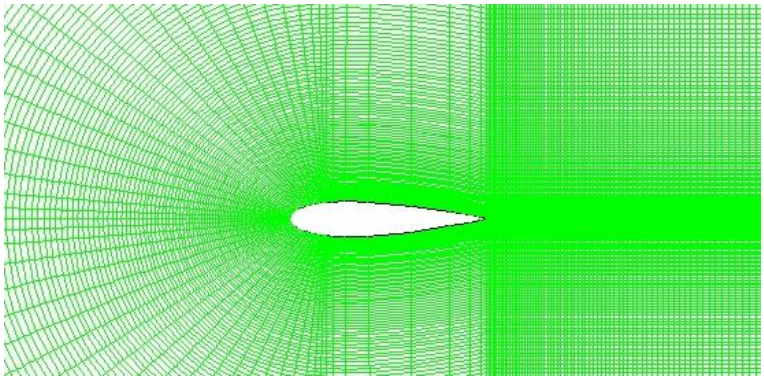

Fig. 3 Denser region near the airfoil

using *KT*. The *KL* equation captures the energy associated with the Tollmien-Schlichting instability in the transition area. The Inverse time scale ω is modeled as epsilon. The inverse time scale in the outer turbulent boundary layer has been proven to lessen the intermittency impact. It more accurately reflects adverse pressure gradients.

4. Numerical analysis

The experimental data from Gerakopulos et al. was used to test the turbulence model on the NACA 0018 airfoil (Gerakopulos *et al.* 2010). First, a surface is produced using 2D airfoil points loaded into ANSYS Design Modeler. After that, the model is loaded into the ANSYS package for meshing. As seen in Fig. 2, a fluid domain forms around the airfoil.

4.1 Domain details

A C-type domain is formed around the airfoil of unit chord length *c*, as shown in Fig. 1. The inlet is 15 c from the airfoil, while the outflow is 20 c. The domain is extended 15c above and below the airfoil to avoid confinement effects. Ansys Meshing is used to mesh the data. A body split approach is used to divide the domain into different zones. High grid density is achieved near

the airfoil by encapsulating a layer of very thin mesh, as shown in Fig. 3. The mesh density steadily increases in the outer zone, coarsening the mesh density as it moves away from the airfoil's surface. A mesh of quad type is generated. The wall *Y*+ is calculated, and the estimated distance is fixed at *Y*+≤1. In order to capture the creation of the separation bubble, it is critical to pay attention to *Y*+.

4.2 Boundary conditions

The relevant study (Gerakopulos *et al*. 2010) states that the same is provided for the turbulence quantities at the boundaries. The no-slip condition enforces *kL*=*kT*=0 for *k-kl-ω* at solid borders. A zero normal gradient condition is employed for omega. The values of *kT* and ω are specified at flow inlets using Eqs. (2) and (3).

$$k_T = \frac{3}{2}(u_\infty I)^2 \tag{10}$$

$$\omega = \frac{C_{\mu,Std} k_T}{\beta \upsilon} \tag{11}$$

I stands for turbulence intensity in the equations above, and β is the eddy viscosity ratio. Earlier investigations supplied the turbulence intensity of 0.1, 0.2, and 0.5, which were used to determine the kinetic energy in this article. The laminar kinetic energy associated with pre-transitional fluctuations is zero at inlets sufficiently removed from solid walls. And the appropriate boundary condition *kL*=0 is specified. For *k-ω* SST, Eqs. (10) and (11) specify the turbulent kinetic energy and frequency.

As the flow is incompressible, a pressure-based solver is used. It is implemented as a SIMPLE pressure velocity coupling. Two turbulence schemes implemented are SST *K-ω* and *k-kl-ω*. The major goal of putting various turbulence models in place is to see which is most effective at capturing flow behavior. Double precision is used to avoid calculating errors. Second-order discretization is used for pressure, momentum, and other factors.

4.3 Grid-independence tests

The grid independence study was carried out after selecting fine mesh settings and varying the number of elements. The grid was varied considering the different number of elements in the domain. The *Cd* was set as the criterion for mesh dependency. The initial 21,620 and 23840 elements in the grid were enough to capture the results. However, the 24,700-element size mesh finally provided an accurate solution, and the comparison of *Cd* is shown in Table 1.

This strategy expanded the grid size while maintaining compatibility with other turbulence models. The mesh size was increased until additional increases in the mesh yielded little difference

Table 1 C_d comparison

Number of Elements	C_d at 4° AoA SST *k*-omega model
21,620	0.0227
23,840	0.0213
24,700	0.0205
25,300	0.0205

in the *Cd* values, as the major goal was to represent the separation bubble. The advantage of utilizing the *SST-k*-omega model is that it is recommended in the literature for improved aerodynamic coefficients. Curvature correction is enabled in Ansys Fluent in this simulation to represent the eddies around the curvature of the airfoil accurately. The results showed that the SST *k*-omega and *k-kl*-omega lift of drag values matched the mesh selected. Flow physics altered when the BL and contour plots were plotted together.

Fine meshing is a better option because all the above errors appeared to be optimized for lift, drag, and efficiency. As a result, the tiny mesh was sufficient for accurately predicting lift, drag, and efficiency in this case study and employed throughout the simulation.

The SST *k*-turbulence model is nearly determined to be more suited for low Reynolds number aeronautical applications. Furthermore, the numerical simulations of the SST model, which corresponds to NACA 0018, have matched the experimental results well. The SST *k*-, on the other hand, could not anticipate the flow transition phenomenon. This phenomenon can be explained by the SST model's fundamental assumption of highly turbulent flow. Except in the post-stall zone, the drag coefficient estimates are typically underestimated.

Therefore, the transition *k-kl-ω* model was employed, and the transition model could predict separation bubbles, as shown in the next sections. Overall, it gave the correct lift and drag coefficient at a low angle of attack but failed to give comparable results after pre-stall angles. In addition, the model managed to predict the transition behavior and increase the model's accuracy. Thus, the flow separation analysis was presented using this turbulence model.

5. Results and discussion

This section discusses the detailed analysis of the experimental and numerical results for the angle of attack ranging from 0° to 18°. The given turbulence models' separation bubble capture and prediction are also compared. The coefficient of pressure plots has explained the flow physics, velocity contours, streamline profiles and a few other plots.

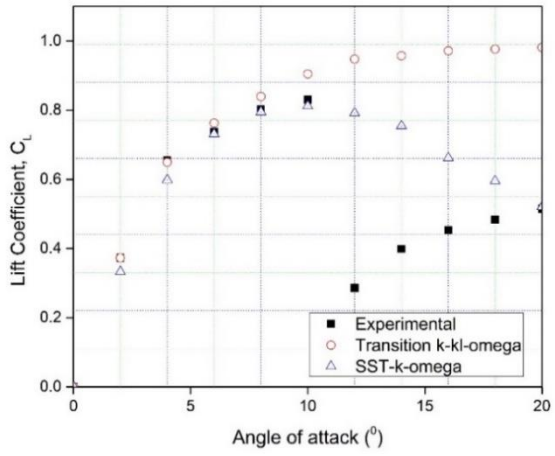

Fig. 4 Lift Coefficients at Re 160,000 compared to experimental results

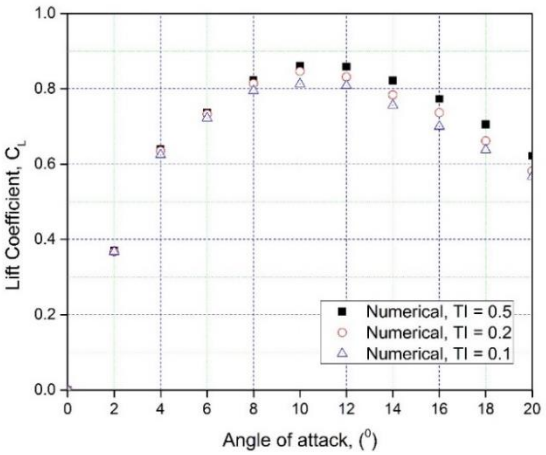

Fig. 5 Lift Coefficients at Re 100,000 compared at different turbulent intensities

5.1 Discussion of the lift coefficient

Lift coefficient information is obtained at various angles of attack at different turbulence models. It is exhibited in Fig. 4 and Fig. 5, respectively. For a given Reynolds number, regular direct development of the lift coefficient with increasing angle of attack happens from α=0° to α≈6°. Then, a more steady development trails this up to the stall point. Finally, a sudden and huge lift coefficient diminishes is observed at the stall angle.

The lift coefficient data of Gerakopulos *et al.* (2010) were compared. They agreed well with the present findings for 0°≤α≤10°; higher lift coefficients are obtained at lower Reynolds numbers for a given angle of attack. The SST model results agree well with the other experimental data set. Unlike full-turbulence models or experimental data, transition-based models anticipate higher flow speeds near the airfoil's top surface, resulting in bigger lift forces.

The results indicate that the agreement between the experimental data and all of the flow model predictions is relatively good for non-stall conditions. Furthermore, as the Reynolds number decreases, the disparity grows. When stall conditions were considered, the Transition k-kl-ω model failed to predict stalls. Full-turbulence models overpredict the lift force under stall conditions because free-stream turbulence encourages the early formation of turbulent boundary layers. Which often prevents flow detachment conditions (surface flow attachment or reattachment is improved in turbulent boundary layer).

Also, the effect of *SST k*-omega turbulent intensity prevails at lower Reynold numbers. Still, at lower angles of attack, the results at all Reynolds numbers show no significant variation in C_L with increasing turbulent intensity. As the attack angle increases towards the pre-stall range, a slightly higher lift is generated at lower turbulent intensity values. The upper limit of the low angle of attack range, and thus the onset of the pre-stall range, shifts to higher angles of attack with increasing Reynolds number.

5.2 Discussion of the pressure coefficient

Fig. 6 shows the surface pressure coefficient *Cp* distribution of the NACA 0018 airfoil at angles of attack of 3° and 10° and Reynolds numbers of 100,000 and 200,000, respectively. When the angle of attack is less than 2.0°, the pressure distribution curve is smooth, and there is no oscillation; however, when the angle of attack equals 2.5°, oscillation is seen in the pressure curve near the trailing edge of the airfoil's upper surface.

Another research (Ghasemi *et al.* 2013) said that while the commencement of oscillation of the pressure curve along the upper trailing edge creeps forward as the AOA increases, the pressure curve's area and amplitude along the airfoil's lower surface remain smooth. Long separation bubbles drastically reduce airfoils' aerodynamic performance and cause unexpected stalling (Choudhry *et al.* 2015).

In addition, it is shown that the airfoil experiences an induced camber effect due to the presence of the Long separation bubbles, the magnitude of which grows with increasing angle of attack. Reducing the bubble extent improves airfoil performance significantly. It causes a progressive trailing-edge stall as the Reynolds number or turbulence increases.

Some non-local approaches to describing transitional flows via RANS equations necessitate the computation of certain boundary layer properties. Transitional and separated flows are predicted using a non-local Laminar Kinetic Energy model in this work. The discontinuous Galerkin method investigates the transitional flows in the T106c turbine cascade and around a NACA0021 airfoil

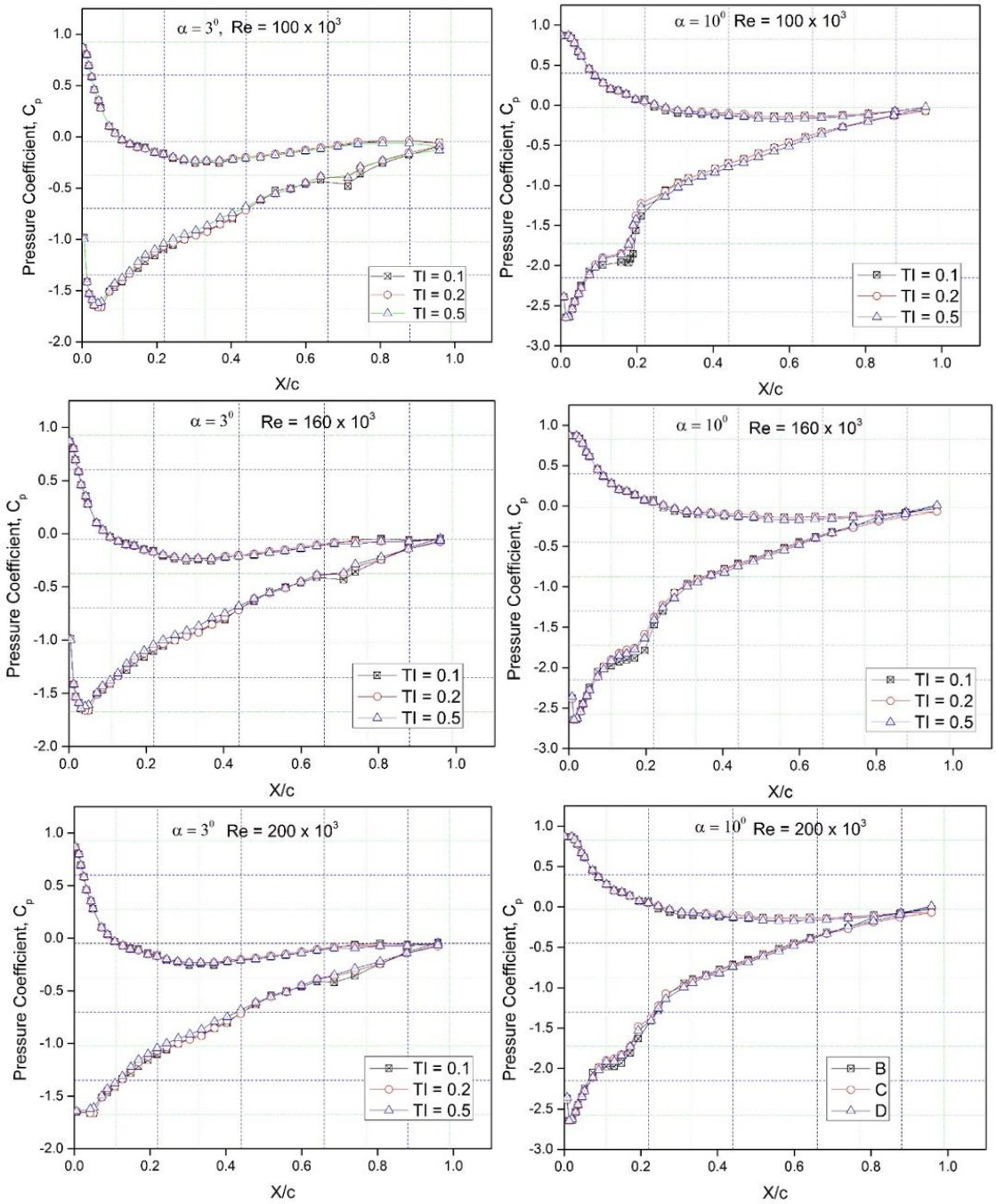

Fig. 6 Pressure coefficient distributions at AoA (2° & 10°) at different Reynolds numbers

(Ferrero *et al.* 2017).

The study's findings reveal that increasing turbulence intensity has no effect on the location of separation bubbles but does result in a shorter bubble length. This is due to a significant upstream

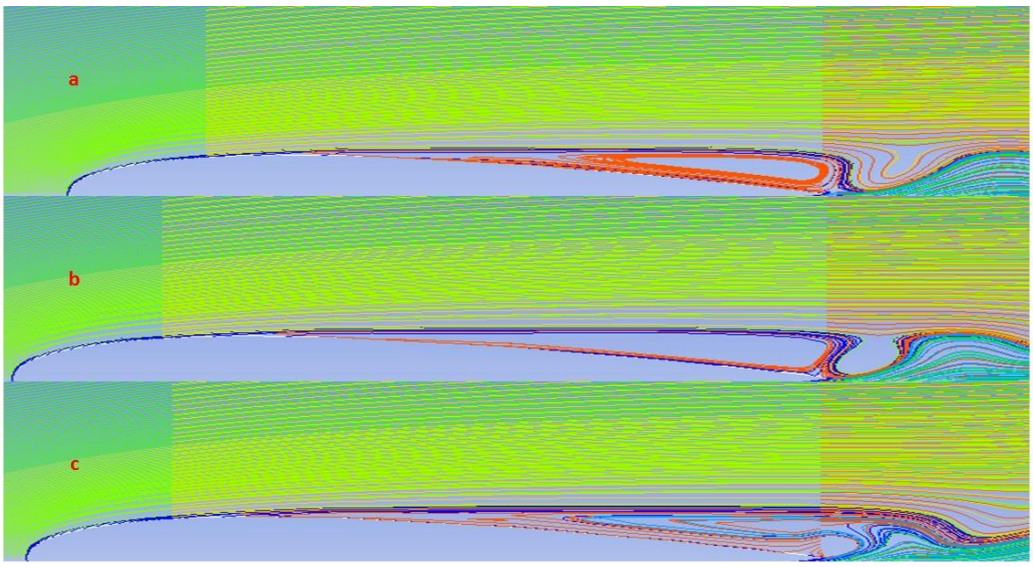

Fig. 7 Separation bubble at the AoA 3°, Re 100,000 (a) TI O.5, (b) TI 0.2, (c) TI 0.1

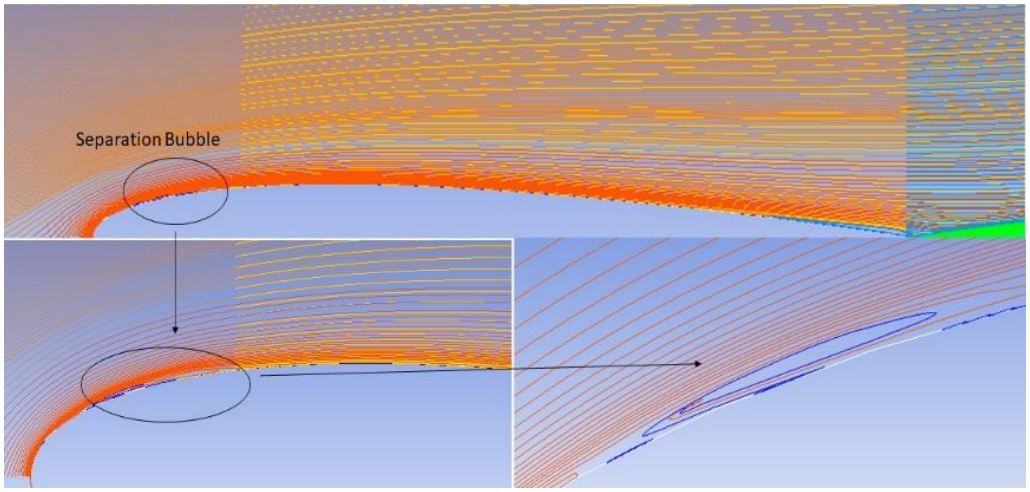

Fig. 8 Separation bubble at an angle of attack of 10° and *Re*=200,000

shift in mean transition and, consequently, mean reattachment. Due to the reduction in local suction over the airfoil at low angles of attack, the reduction in separation bubble length causes a minor reduction in airfoil lift. It should be emphasized that the effect was more noticeable at lower Reynolds numbers. As Reynolds numbers increased, the influence of turbulent intensity became less noticeable.

Regarding the accuracy of the two models, SST-K-OMEGA failed to anticipate transition behavior and separation bubble. Even with a revised grid, the production of separation bubbles and other instabilities that occur in low Reynolds number flows are not represented. As a result, SST K-ω is more accurate for totally turbulent flow but not nearly sufficient for transition simulation, as indicated.

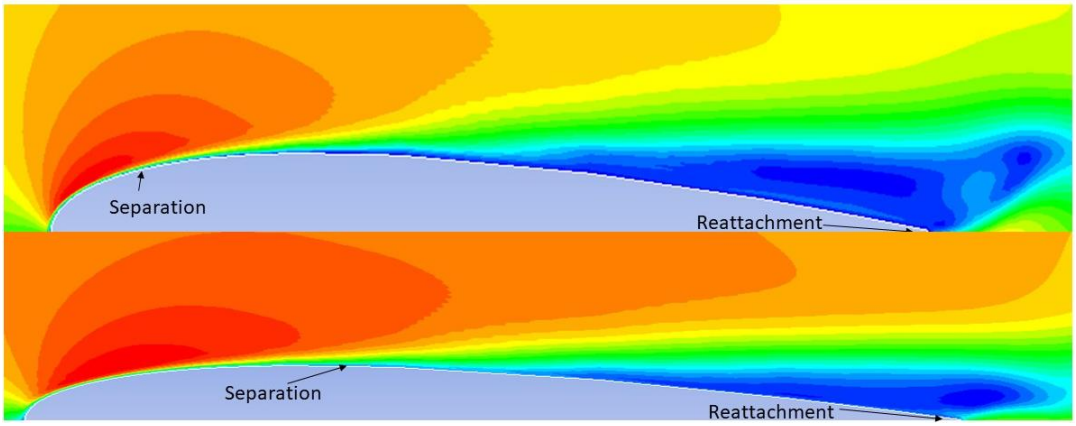

Fig. 9 Flow separation and reattachment at an angle of attack 8° and 6° respectively

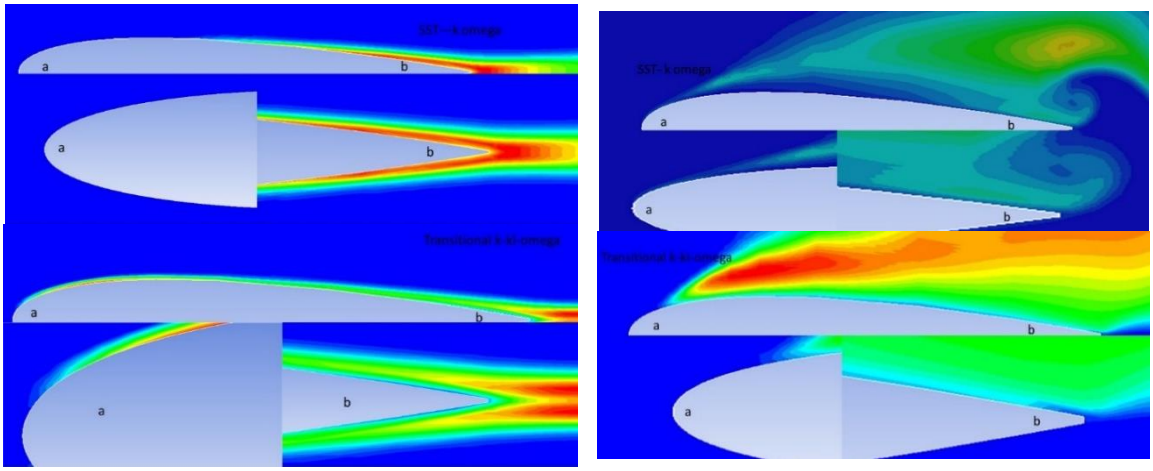

Fig. 10 Turbulent kinetic energy of two different turbulence models at AoA 0° (left) and 18° at *Re*=160,000

The Cp graphs for *k-kl-* in Fig. 6 reveal the presence of a bubble but do not accurately predict flow behavior. The initial laminar separation at the airfoil's trailing edge was accurately captured. However, as seen in the simulation findings, the reattachment was underestimated. Fig. 7 demonstrates that with a 3° angle of attack, the laminar separation bubble forms at approximately 0.65 chord and extends to 0.65 chord. At 0.85 chord, the turbulent reattachment occurs, where the flow reconnects with the surface, as shown in Figs. 8 and 9.

The large turbulent kinetic energy and the large turbulent viscosity predicted by the *SST-k-*omega model were well predicted, as shown in Fig. 10. The presence of the model in the vicinity of the airfoil results in enhanced transversal diffusion of momentum that is most noticeable at the airfoil's upper surface, resulting in a significant reduction in the magnitude of the flow speed and an alteration in the direction of the resulting flow direction. However, to a certain extent, the Transition *k-kl*-omega model described the premature flow detachment conditions essential for the adequate prediction of separation.

6. Conclusions

The parametric study results show that increasing the level of free-stream turbulence intensity results in a reduction in separation bubble length. Primarily due to an upstream shift in mean transition and, as a result, mean reattachment as the level of free-stream turbulence intensity is increased. At low angles of attack, the reduction in separation bubble length results in a minor drop in airfoil lift due to the reduction in local suction over the airfoil caused by the reduction in separation bubble length. As a result of this current simulation, the *K-ω SST* provides good results for estimating lift coefficients, with only minor variations at higher angles of attack. However, the Transition *K-kl-ω* did not predict a stall. Both models indicate a little development of the separating bubble but fall short of capturing it completely. In external aerodynamic instances where the flow is entirely turbulent, *K-ω SST* has produced good results in previous studies. At a low AoA (6°), the *k-kl-ω* produced extremely positive results. It was also used to predict separation bubbles with high accuracy. However, there were some over-predictions in the flow reattachment locations over the airfoil when using the transition k-*kl*-model. The *Cp* plots demonstrated that the model produced results that were more similar to the experimental results.

Acknowledgements

This research was funded by Universiti Sains Malaysia Bridging GRA Grant (304/PAERO/6316608). The authors confirm that the data supporting the findings of this study are available within the article. The authors declare no conflict of interest.

References

Aftab, S.M.A., Mohd Rafie, A.S., Razak, N.A. and Ahmad, K.A. (2016), "Turbulence model selection for low reynolds number flows", *PloS one*, **11**(4), e0153755. https://doi.org/10.1371/journal.pone.0153755.

Carmichael, B.H. (1981), *Low Reynolds Number Airfoil Survey*, Volume 1 (No. NASA-CR-165803-VOL-1).

Choudhry, A., Arjomandi, M. and Kelso, R. (2015), "A study of long separation bubble on thick airfoils and its consequent effects", *Int. J. Heat Fluid Flow*, **52**, 84-96. https://doi.org/10.1016/j.ijheatfluidflow.2014.12.001.

Drela, M. (1989), "XFOIL: An analysis and design system for low Reynolds number airfoils", *Low Reynolds Number Aerodynamics*, Springer.

Ferrero, A., Larocca, F. and Bernaschek, V. (2017), "Unstructured discretisation of a non-local transition model for turbomachinery flows", *Adv. Aircraft Spacecraft Sci.*, **4**(5), 555. https://doi.org/10.12989/aas.2017.4.5.555.

Gerakopulos, R., Boutilier, M.S. and Yarusevych, S. (2010), "Aerodynamic characterisation of a NACA 0018 airfoil at low Reynolds numbers", *AIAA*, 4629. https://doi.org/10.2514/6.2010-4629.

Ghasemi, E., McEligot, D.M., Nolan, K.P., Crepeau, J., Tokuhiro, A. and Budwig, R.S. (2013), "Entropy generation in a transitional boundary layer region under the influence of free-stream turbulence using transitional RANS models and DNS", *Int. Commun. Heat Mass Transf.*, **41**, 10-16. https://doi.org/10.1016/j.icheatmasstransfer.2012.11.005.

Herbert-Acero, J.F., Probst, O., Rivera-Solorio, C.I., Castillo-Villar, K.K. and Méndez-Díaz, S. (2015), "An extended assessment of fluid flow models for the prediction of two-dimensional steady-state airfoil aerodynamics", *Math. Prob. Eng.*, **2015**, Article ID 854308. https://doi.org/10.1155/2015/854308.

Istvan, M., Kurelek, J. and Yarusevych, S. (2016), "Effects of free-stream turbulence intensity on laminar separation bubbles", *46th AIAA Fluid Dynamics Conference*, Washington D.C., June.

Jones, G., Santer, M. and Papadakis, G. (2018), "Control of low Reynolds number flow around an airfoil using periodic surface morphing: A numerical study", *J. Fluid. Struct.*, **76**, 95-115. https://doi.org/10.1016/j.jfluidstructs.2017.09.009.

Kamada, Y., Maeda, T., Murata, J. and Nishida, Y. (2016), "Effect of turbulent inflows on airfoil performance for a Horizontal Axis Wind Turbine at low Reynolds numbers (Part II: Dynamic pressure measurement)", *Energy*, **112**, 574-587. https://doi.org/10.1016/j.energy.2016.06.126.

Kojima, R., Nonomura, T., Oyama, A. and Fujii, K. (2013), "Large-eddy simulation of low-Reynolds-number flow over thick and thin NACA airfoils", *J. Aircraft*, **50**(1), 187-196. https://doi.org/10.2514/1.C031849.

Lachenal, X., Daynes, S. and Weaver, P.M. (2013), "Review of morphing concepts and materials for wind turbine blade applications", *Wind Energy*, **16**(2), 283-307. https://doi.org/10.1002/we.531.

Menter, F.R., Kuntz, M. and Langtry, R. (2003), "Ten years of industrial experience with the SST turbulence model", *Turbul. Heat Mass Transf.*, **4**(1), 625-632.

Mueller, T.J. and DeLaurier, J.D. (2003), "Aerodynamics of small vehicles", *Ann. Rev. Fluid Mech.*, **35**(1), 89-111. https://doi.org/10.1146/annurev.fluid.35.101101.161102.

O'meara, M. and Mueller, T. (1987), "Laminar separation bubble characteristics on an airfoil at low Reynolds number", *AIAA J.*, **25**(8), 1033-1041. https://doi.org/10.2514/3.9739.

Rogowski, K., Hansen, M.O. and Maroński, R. (2018), "Steady and unsteady analysis of NACA 0018 airfoil in vertical-axis wind turbine", *J. Theor. Appl. Mech.*, **56**(1), 203-212. https://doi.org/10.15632/jtam-pl.56.1.203.

Rogowski, K., Królak, G. and Bangga, G. (2021), "Numerical study on the aerodynamic characteristics of the NACA 0018 airfoil at low Reynolds number for darrieus wind turbines using the transition SST model", *Proc.*, **9**(3), 477. https://doi.org/10.3390/pr9030477.

Shen, X., Avital, E., Paul, G., Rezaienia, M.A., Wen, P. and Korakianitis, T. (2016), "Experimental study of surface curvature effects on aerodynamic performance of a low Reynolds number airfoil for use in small wind turbines", *J. Renew. Sustain. Energy*, **8**(5), 053303. https://doi.org/10.1063/1.4963236.

Theofilis, V. and Sherwin, S.J. (2001), "Global instabilities in trailing-edge laminar separated flow on a NACA 0012 Airfoil", *15th ISABE (International Symposium on Airbreathing Engines)*, Bangalore, India, September.

Yarusevych, S., Sullivan, P.E. and Kawall, J.G. (2006), "Coherent structures in an airfoil boundary layer and wake at low Reynolds numbers", *Phys. Fluid.*, **18**(4), 044101. https://doi.org/10.1063/1.2187069.

Zhou, W., Ning, Z., Li, H. and Hu, H. (2017), "An experimental investigation on rotor-to-rotor interactions of small UAV", *35th AIAA Applied Aerodynamics Conference*, Denver, Colorado, June.

AP